First measurement of the masses of the $\Upsilon_1(1D)$ and $\Upsilon_3(1D)$ states and the energy dependence of the cross sections for $e^+e^- \to \Upsilon_J(1D)\eta$ and $e^+e^- \to \Upsilon_J(1D)\pi^+\pi^-$

M. Abumusabh, I. Adachi, K. Adamczyk, A. Aggarwal, H. Ahmed, Y. Ahn, M. Akdag, N. Akopov, S. Alghamdi, M. Alhakami, N. Althubiti, K. Amos, M. Angelsmark, N. Anh Ky, C. Antonioli, K. Arai, H. Atmacan, T. Aushev, V. Aushev, R. Ayad, V. Babu, H. Bae, N. K. Baghel, S. Bahinipati, P. Bambade, Sw. Banerjee, M. Barrett, M. Bartl, J. Baudot, A. Baur, A. Beaubien, F. Becherer, J. Becker, G. F. Benfratello, J. V. Bennett, F. U. Bernlochner, V. Bertacchi, M. Bertemes, E. Bertholet, M. Bessner, S. Bettarini, V. Bhardwaj, B. Bhuyan, F. Bianchi, T. Bilka, A. Biswas, D. Biswas, A. Bobrov, D. Bodrov, A. Bondar, G. Bonvicini, A. Boschetti, A. Bozek, M. Bračko, P. Branchini, R. A. Briere, T. E. Browder, A. Budano, Q. Campagna, M. Campajola, M. Carminati, G. Casarosa, C. Cecchi, M.-C. Chang, P. Cheema, L. Chen, B. G. Cheon, C. Cheshta, H. Chetri, K. Chilikin, K. Chirapatpimol, H.-E. Cho, K. Cho, S.-J. Cho, S.-K. Choi, S. Choudhury, S. Chutia, J. A. Colorado-Caicedo, I. Consigny, L. Corona, H. Crotte Ledesma, S. Cuccuini, J. X. Cui, E. De La Cruz-Burelo, S. A. De La Motte, G. De Nardo, G. De Pietro, R. de Sangro, M. Destefanis, S. Dey, R. Dhayal, A. Di Canto, J. Dingfelder, Z. Doležal, X. Dong, M. Dorigo, K. Dugic, G. Dujany, P. Ecker, D. Epifanov, J. Eppelt, R. Farkas, P. Feichtinger, T. Ferber, T. Fillinger, C. Finck, G. Finocchiaro, F. Forti, B. G. Fulsom, A. Gabrielli, A. Gale, R. Garg, A. Garmash, G. Gaudino, V. Gaur, V. Gautam, P. Gebeline, A. Gellrich, G. Ghevondyan, D. Ghosh, G. Giakoustidis, R. Giordano, A. Giri, P. Gironella Gironell, B. Gobbo, R. Godang, O. Gogota, W. Gradl, E. Graziani, D. Greenwald, K. Gudkova, Y. Han, K. Hayasaka, H. Hayashii, S. Hazra, C. Hearty, M. T. Hedges, A. Heidelbach, G. Heine, I. Heredia de la Cruz, T. Higuchi, M. Hoek, M. Hohmann, R. Hoppe, P. Horak, C.-L. Hsu, T. Humair, T. Iijima, K. Inami, N. Ipsita, A. Ishikawa, R. Itoh, M. Iwasaki, D. Jacobi, W. W. Jacobs, E.-J. Jang, Q. P. Ji, S. Jia, Y. Jin, A. Johnson, K. K. Joo, H. Kakuno, K. H. Kang, G. Karyan, T. Kawasaki, C. Ketter, C. Kiesling, C. Kim, D. Y. Kim, H. Kim, J.-Y. Kim, K.-H. Kim, H. Kindo, K. Kinoshita, P. Kodyš, T. Koga, S. Kohani, A. Korobov, S. Korpar, E. Kovalenko, R. Kowalewski, M. Krein, P. Križan, P. Krokovny, T. Kuhr, D. Kumar, R. Kumar, K. Kumara, T. Kunigo, Y.-J. Kwon, S. Lacaprara, Y.-T. Lai, T. Lam, J. S. Lange, T. S. Lau, R. Leboucher, H. Lee, M. J. Lee, C. Lemettais, P. Leo, C. Li, L. K. Li, Q. M. Li, S. X. Li, W. Z. Li, Y. Li, Y. B. Li, Y. P. Liao, J. Libby, J. Lin, V. Lisovskyi, C. Liu, Q. Y. Liu, Z. Q. Liu, D. Liventsev, S. Longo, A. Lozar, C. Lyu, J. L. Ma, Y. Ma, M. Maggiora, S. P. Maharana, R. Maiti, G. Mancinelli, E. Manoni, M. Mantovano, D. Marcantonio, S. Marcello, M. Marfoli, C. Marinas, C. Martellini, A. Martens, T. Martinov, L. Massaccesi, M. Masuda, S. K. Maurya, M. Maushart, J. A. McKenna, Z. Mediankin Gruberová, R. Mehta, F. Meier, D. Meleshko, M. Merola, C. Miller, M. Mirra, K. Miyabayashi, H. Miyake, R. Mizuk, S. Moneta, A. L. Moreira de Carvalho, H.-G. Moser, A. Mubarak, N. Mudgal, Th. Muller, H. Murakami, R. Mussa, M. Nakao, Y. Nakazawa, M. Naruki, Z. Natkaniec, A. Natochii, M. Nayak, M. Neu, M. Niiyama, S. Nishida, R. Nomaru, S. Ogawa, H. Ono, Y. Onuki, I. Ostrowski, F. Otani, S. Pardi, J. Park, K. Park, S.-H. Park, A. Passeri, S. Patra, T. K. Pedlar, R. Pestotnik, M. Piccolo, L. E. Piilonen, P. L. M. Podesta-Lerma, T. Podobnik, L. Polat, A. Prakash, V. Prasad, S. Prell, E. Prencipe, M. T. Prim, S. Privalov, P. Rados, S. Raiz, K. Ravindran, J. U. Rehman, M. Reif, S. Reiter, M. Remnev, D. Ricalde Herrmann, I. Ripp-Baudot, G. Rizzo, S. H. Robertson, J. M. Roney, A. Rostomyan, N. Rout, G. Russo, S. Saha, S. Sandilya, C. Santos, V. Savinov, B. Scavino, J. Schmitz, S. Schneider, G. Schnell, K. Schoenning, C. Schwanda, Y. Seino, K. Senyo, J. Serrano, C. Sfienti, W. Shan, C. P. Shen, X. D. Shi, T. Shillington, J.-G. Shiu, D. Shtol, B. Shwartz, A. Sibidanov, F. Simon, J. B. Singh, J. Skorupa, A. Soffer, A. Sokolov, E. Solovieva, W. Song, S. Spataro, K. Špenko, B. Spruck, M. Starič, P. Stavroulakis, S. Stefkova, R. Stroili, M. Sumihama, M. Takizawa, U. Tamponi, S. Tanaka, K. Tanida, F. Testa, D. V. Thanh, T. Tien Manh, O. Tittel, R. Tiwary, E. Torassa, F. F. Trantou, I. Tsaklidis, M. Uchida, I. Ueda, E. Uenlue, T. Uglov, K. Unger, Y. Unno, K. Uno, S. Uno, R. van Tonder, K. E. Varvell, M. Veronesi, V. S. Vismaya,

L. Vitale, V. Vobbilisetti, R. Volk, S. Wallner, M.-Z. Wang, A. Warburton, M. Watanabe, S. Watanuki, C. Wessel, Y. Xie, X. P. Xu, B. D. Yabsley, S. Yamada, W. Yan, W. P. Yan, J. Yelton, K. Yi, J. H. Yin, K. Yoshihara, C. Z. Yuan, J. Yuan, L. Yuan, Y. Yusa, L. Zani, M. Zeyrek, B. Zhang, X. Zhao, V. Zhilich, J. S. Zhou, Q. D. Zhou, L. Zhu, and R. Žlebčík
(The Belle and Belle II Collaborations)

We study the processes $e^+e^- \to \Upsilon_J(1D)\eta$ and $e^+e^- \to \Upsilon_J(1D)\pi^+\pi^-$ at center-of-mass energies $\sqrt{s}$=(10.73 – 11.02) GeV using a 142.5 fb^{-1} data sample, including 122 fb^{-1} near the $\Upsilon(10860)$ peak ($\sqrt{s} = 10.866$ GeV), collected with the Belle detector at the KEKB asymmetric-energy e^+e^- collider. From the peak sample, the products of Born cross section times branching fraction are obtained for $\sigma_{\rm Born}(e^+e^- \to \Upsilon_J(1D)\eta)$ or $\sigma_{\rm Born}(e^+e^- \to \Upsilon_J(1D)\pi^+\pi^-)$ and $\mathcal{B}(\Upsilon_J(1D) \to \chi_{b1}\gamma)$ or $\mathcal{B}(\Upsilon_J(1D) \to \chi_{b2}\gamma)$ for each $\Upsilon_J(1D)$ state. The corresponding branching fractions for $\Upsilon(10860)$ decays are also obtained. The significances of the $\Upsilon_1(1D)$, $\Upsilon_2(1D)$, and $\Upsilon_3(1D)$ signals are 4.8σ, $>10\sigma$, and 3.0σ, respectively, including systematic uncertainties. The mass for $\Upsilon_2(1D)$ is measured to be $(10167.0\pm1.0\pm0.2)$ MeV/c^2, where the first and second uncertainties are statistical and systematic. The mass splittings $\Delta m_{12} = m(\Upsilon_2(1D)) - m(\Upsilon_1(1D))$ and $\Delta m_{23} = m(\Upsilon_3(1D)) - m(\Upsilon_2(1D))$ are $(11.8 \pm 1.5 \pm 0.4)$ MeV/c^2 and $(7.6 \pm 2.4 \pm 0.6)$ MeV/c^2, respectively. We determine the energy dependence of the cross sections for $e^+e^- \to \Upsilon_J(1D)\eta$ and $e^+e^- \to \Upsilon_J(1D)\pi^+\pi^-$ for the $\Upsilon_1(1D)$, $\Upsilon_2(1D)$, and $\Upsilon_3(1D)$ states, combined.

As a prominent member of the heavy quarkonium family, bottomonium is an ideal probe for the nonperturbative behavior of quantum chromodynamics [1–4]. To date, only one D-wave bottomonium state, $\Upsilon_2(1D)$, has been observed, by CLEO and BaBar [5, 6]. The relativized quark model, nonrelativistic constituent quark model, screened potential model, and the modified relativized quark model with a screening effect have predicted the mass splittings of the $\Upsilon_J(1D)$ [7–10]. However, the states $\Upsilon_1(1D)$ and $\Upsilon_3(1D)$ have not yet been observed.

Within the hadronic loop mechanism, the branching fractions for $\Upsilon(10860) \to \Upsilon_J(1D)\eta$, $\Upsilon(11020) \to \Upsilon_J(1D)\eta$, and $\Upsilon(10860) \to \Upsilon_J(1D)\pi^+\pi^-$ range in magnitude from 10^{-4} to 10^{-3} [11–13]. In a 121.4 fb^{-1} sample at $\sqrt{s} = 10.866$ GeV, Belle studied $e^+e^- \to \Upsilon_J(1D)\eta$ and $e^+e^- \to \Upsilon_J(1D)\pi^+\pi^-$ in the recoil mass spectra of η and $\pi^+\pi^-$ [14, 15], where the $\Upsilon_1(1D)$, $\Upsilon_2(1D)$, and $\Upsilon_3(1D)$ states were treated as a single component or with fixed mass splittings. In this work, we separate $\Upsilon_1(1D)$, $\Upsilon_2(1D)$, and $\Upsilon_3(1D)$ states through exclusive reconstruction, applying a kinematic constraint, and performing a three-dimensional (3D) fit. To date, there are no reported experimental results for $e^+e^- \to \Upsilon_J(1D)\eta$ and $e^+e^- \to \Upsilon_J(1D)\pi^+\pi^-$ in the energy region around the $\Upsilon(11020)$ resonance.

In this Letter, we measure the cross sections for $e^+e^- \to \Upsilon_J(1D)\eta$ and $e^+e^- \to \Upsilon_J(1D)\pi^+\pi^-$ using Belle data at $\sqrt{s}$ from 10.73 to 11.02 GeV. We report first evidence for the $\Upsilon_1(1D)$ and $\Upsilon_3(1D)$ states, as well as measurements of the $\Upsilon_J(1D)$ masses. For the energy point at $\sqrt{s} = 10.866$ GeV, we determine the product of the Born cross section for $e^+e^- \to \Upsilon_J(1D)\eta$ ($e^+e^- \to \Upsilon_J(1D)\pi^+\pi^-$) and the branching fraction of $\Upsilon_J(1D) \to \chi_{b1,b2}\gamma$. The corresponding branching fractions for the $\Upsilon(10860)$ decays are also found.

The data reported here were recorded by the Belle detector [16, 17] at the KEKB asymmetric-energy e^+e^- collider [18, 19]. We use ≈1 fb^{-1} taken at each of 18 center-of-mass (c.m.) energies in the range 10.73 GeV – 11.02 GeV (energy scan data) and a 122 fb^{-1} sample collected at the $\Upsilon(10860)$, $\sqrt{s}$=10865.8 MeV ($\Upsilon(10860)$ on-resonance data). Thus, there are 19 energy points in total at which we measure cross sections for $e^+e^- \to \Upsilon_J(1D)\eta$ and $\Upsilon_J(1D)\pi^+\pi^-$. A detailed description of the Belle detector can be found in Refs. [16, 17].

We generate signal Monte Carlo (MC) events with c.m. energies from 10.73 to 11.02 GeV using the EVTGEN generator [20] to determine the reconstruction efficiencies and signal shapes. Initial-state radiation (ISR) at next-to-leading order precision in quantum electrodynamics is simulated with PHOKHARA [21]. For $e^+e^- \to \Upsilon_J(1D)\eta$, the polar angle of the η in the e^+e^- c.m. system (θ_η) is distributed according to $(1 + \cos^2\theta_\eta)$, $(1 - \frac{1}{7}\cos^2\theta_\eta)$, and $(1 + \cos^2\theta_\eta)$ for $\Upsilon_1(1D)\eta$, $\Upsilon_2(1D)\eta$, and $\Upsilon_3(1D)\eta$ production, respectively. For $e^+e^- \to \Upsilon_J(1D)\pi^+\pi^-$, the polar angle of the $\pi^+\pi^-$ system in the e^+e^- c.m. system ($\theta_{\pi^+\pi^-}$) is distributed uniformly. Generic MC samples of $e^+e^- \to q\bar{q}$ ($q = u, d, s, c$) with the KKMC [22] and PYTHIA packages and $\Upsilon(10860) \to B^{(*)}_{(s)}\bar{B}^{(*)}_{(s)}$ produced with 4 times the luminosity of the data are used to estimate backgrounds. The simulated events are processed with a detector simulation based on GEANT3 [23].

We reconstruct the decay chains [7–10]

$$e^+e^- \to \Upsilon_J(1D)\eta,\ e^+e^- \to \Upsilon_J(1D)\pi^+\pi^-,$$
$$\eta \to \gamma\gamma,\ \eta \to \pi^+\pi^-\pi^0,$$
$$\Upsilon_1(1D) \to \chi_{b1}\gamma,\ \Upsilon_2(1D) \to \chi_{b1,b2}\gamma,\ \Upsilon_3(1D) \to \chi_{b2}\gamma,$$
$$\chi_{b1,b2} \to \Upsilon(1S)\gamma,\ \text{and}\ \Upsilon(1S) \to \ell^+\ell^-\ (\ell = \mu \text{ or } e).$$

The χ_{b0} is not included due to a small branching fraction for $\chi_{b0} \to \Upsilon(1S)\gamma$ [24–26]. Event selection and criteria for tracks and particle identification follow the methods

used in Refs. [27, 28].

We require the energies of photons from π^0 and η candidates to be greater than 50 MeV and 100 MeV, respectively. The signal regions for $\pi^0 \to \gamma\gamma$, $\eta \to \gamma\gamma$, and $\eta \to \pi^+\pi^-\pi^0$ are $110 < M(\gamma\gamma) < 150$ MeV/c^2 ($\pm 2.5\sigma$), $0.51 < M(\gamma\gamma) < 0.58$ GeV/c^2 ($\pm 2.5\sigma$), and $0.535 < M(\pi^+\pi^-\pi^0) < 0.560$ GeV/c^2 ($\pm 2.5\sigma$), respectively, where the symbol M denotes invariant mass and the σ is the mass resolution.

The $\Upsilon(1S)$ signal regions are $9.15 < M(e^+e^-) < 9.66$ GeV/c^2 and $9.26 < M(\mu^+\mu^-) < 9.66$ GeV/c^2 (approximately $\pm 2.5\sigma$).

Photon pairs remaining in the event are used to reconstruct $\chi_{b1,b2}$ and $\Upsilon_J(1D)$ candidates. The photon with the higher energy (γ_H) in the e^+e^- c.m. frame is used to reconstruct $\chi_{b1,b2} \to \Upsilon(1S)\gamma$, and the other ($\gamma_L$) to reconstruct $\Upsilon_J(1D) \to \chi_{b1,b2}\gamma$. To calibrate the photon energy resolution function, three control channels $D^{*0} \to D^0\gamma$, $\pi^0 \to \gamma\gamma$, and $\eta \to \gamma\gamma$ are used [29].

We require the numbers of charged tracks to be two, four, and four in the channels $e^+e^- \to \Upsilon_J(1D)\eta(\to \gamma\gamma)$, $e^+e^- \to \Upsilon_J(1D)\eta(\to \pi^+\pi^-\pi^0)$, and $e^+e^- \to \Upsilon_J(1D)\pi^+\pi^-$, respectively. For $e^+e^- \to \Upsilon_J(1D)\pi^+\pi^-$, background from $\gamma \to e^+e^-$ conversions is removed by requiring $\cos\theta_{\pi^+\pi^-} < 0.95$, where $\theta_{\pi^+\pi^-}$ is the angle between π^+ and π^- in the laboratory frame.

To reduce backgrounds with additional particles in the final state, a 5C kinematic fit using KFIT [30] is performed, where the four-momentum of the final state system is constrained to match the initial e^+e^- c.m. system, and the invariant mass of the lepton pair is constrained to the $\Upsilon(1S)$ nominal mass [26]. The $\chi^2_{\rm 5C}/n_{\rm dof}$ value of the 5C fit is required to be less than 20 which retains 98% of the signal. In events with multiple candidates, only the candidate with the smallest value of $\chi^2_{\rm 5C}$ is retained. The fractions of selected events with multiple candidates are found in signal MC to be 8%, 2%, and 1% for $e^+e^- \to \Upsilon_J(1D)\eta(\to \gamma\gamma)$, $e^+e^- \to \Upsilon_J(1D)\eta(\to \pi^+\pi^-\pi^0)$, and $e^+e^- \to \Upsilon_J(1D)\pi^+\pi^-$, respectively. These values are consistent with the multiple candidate rates observed in the data. The fractions of correctly reconstructed candidates in $e^+e^- \to \Upsilon_J(1D)\eta(\to \gamma\gamma)$, $e^+e^- \to \Upsilon_J(1D)\eta(\to \pi^+\pi^-\pi^0)$, and $e^+e^- \to \Upsilon_J(1D)\pi^+\pi^-$ are found to be 94%, 97%, and 98%, respectively.

For the data at $\sqrt{s} = 10.866$ GeV, we simultaneously fit to the $e^+e^- \to \Upsilon_J(1D)\eta$ and $e^+e^- \to \Upsilon_J(1D)\pi^+\pi^-$ channels, where the masses of the $\Upsilon_J(1D)$ are constrained to be the same. For $e^+e^- \to \Upsilon_J(1D)\eta$ or $e^+e^- \to \Upsilon_J(1D)\pi^+\pi^-$, we perform a 3D unbinned extended maximum-likelihood fit to the $M'(\ell^+\ell^-\gamma_H) = M(\ell^+\ell^-\gamma_H) - M(\ell^+\ell^-) + m(\Upsilon(1S))$ ($\chi_{b1,b2}$ mass), $\Delta M = M(\ell^+\ell^-\gamma_H\gamma_L) - M(\ell^+\ell^-\gamma_H)$ (mass difference between $\chi_{b1,b2}$ and $\Upsilon_J(1D)$), and $M'_{\rm rec}(\eta) = M_{\rm rec}(\eta) + M(\gamma\gamma, \pi^+\pi^-\pi^0) - m(\eta)$ or $M_{\rm rec}(\pi^+\pi^-)$ ($\Upsilon_J(1D)$ mass) distributions before the kinematic fit to extract signal yields. Hereinafter, the variables $M_{\rm rec}$ and m denote the recoil mass and the nominal mass [26]. The magnitude of the maximum correlation coefficient among the above three observables is 1% from simulation. The fitting function is a sum of the following components: 3D signal peaks and corresponding combinatorial backgrounds for $\Upsilon_1(1D) \to \chi_{b1}\gamma$, $\Upsilon_2(1D) \to \chi_{b1}\gamma$, $\Upsilon_2(1D) \to \chi_{b2}\gamma$, and $\Upsilon_3(1D) \to \chi_{b2}\gamma$ in $M'(\ell^+\ell^-\gamma_H)$, ΔM, $M'_{\rm rec}(\eta)$ or $M_{\rm rec}(\pi^+\pi^-)$, respectively. The 3D signal and background probability density functions (PDFs) are each the product of the three 1D PDFs.

The signal shapes in $M'(\ell^+\ell^-\gamma_H)$ and ΔM are each described by a crystal ball (CB) function [31]. The signal shapes in $M'_{\rm rec}(\eta)$ and $M_{\rm rec}(\pi^+\pi^-)$ are described by double Gaussian functions. Except for the masses of the $\Upsilon_J(1D)$ states, all parameters are fixed according to signal MC simulations. A first-order polynomial function with free parameters is used to describe the combinatorial background. The justification for using this polynomial is verified through the control channels $e^+e^- \to \Upsilon(2S)(\to \chi_{b1,b2}\gamma)\eta$ and $e^+e^- \to \Upsilon(2S)(\to \chi_{b1,b2}\gamma)\pi^+\pi^-$. The yield ratio $N^{\rm sig}(\eta \to \gamma\gamma)/N^{\rm sig}(\eta \to \pi^+\pi^-\pi^0)$ is fixed at 4.2 in the 3D fit according to the products of branching fractions and efficiencies. The ratio of the yields $N^{\rm sig}(\Upsilon_2(1D) \to \chi_{b1}\gamma)/N^{\rm sig}(\Upsilon_2(1D) \to \chi_{b2}\gamma)$ in $e^+e^- \to \Upsilon_J(1D)\eta$ and $e^+e^- \to \Upsilon_J(1D)\pi^+\pi^-$ is floated as a common parameter.

Fit projections for the signal region are shown in Fig. 1. The signal yields are listed in Table I. The statistical significances of the signals are calculated from the difference of the logarithmic likelihoods [32], $-2\ln(\mathcal{L}_0/\mathcal{L}_{\rm max})$, where $\mathcal{L}_0$ and $\mathcal{L}_{\rm max}$ are the maximized likelihoods without and with a signal component, respectively, taking into account the difference in the number of degrees of freedom (Δndf = 4 for the $\Upsilon_2(1D)$ and 3 for the $\Upsilon_{1,3}(1D)$). The statistical significances are 5.1σ, $>10\sigma$, and 3.1σ for $\Upsilon_1(1D)$, $\Upsilon_2(1D)$, and $\Upsilon_3(1D)$, respectively, and the significances including systematic uncertainties are 4.8σ, $>10\sigma$, and 3.0σ. We varied the fit configurations over all additive systematic variations (discussed below), and conservatively took the lowest values as the significances with systematics included.

The mass of $\Upsilon_2(1D)$ is found to be $(10167.0 \pm 1.0 \pm 0.2)$ MeV/c^2. The first and second uncertainties are statistical and systematic, throughout this paper. The mass difference from the world average mass of (10163.7 ± 1.4) MeV/c^2 [26] is 1.8σ. The mass splittings $\Delta m_{12} = m(\Upsilon_2(1D)) - m(\Upsilon_1(1D))$ and $\Delta m_{23} = m(\Upsilon_3(1D)) - m(\Upsilon_2(1D))$ are $(11.8 \pm 1.5 \pm 0.4)$ MeV/c^2 and $(7.6 \pm 2.4 \pm 0.6)$ MeV/c^2, respectively. The branching fraction ratio $\mathcal{B}(\Upsilon_2(1D) \to \chi_{b2}\gamma)/\mathcal{B}(\Upsilon_2(1D) \to \chi_{b1}\gamma)$ is $0.66 \pm 0.27 \pm 0.15$, which is consistent with the prediction of $\approx$0.3 in Refs. [7–10]. The distribution of $M(\pi^+\pi^-)$ in $e^+e^- \to \Upsilon_J(1D)\pi^+\pi^-$ is shown in the Supplemental Material [33].

For each $\Upsilon_J(1D)$ state and $\Upsilon_J(1D)$ radiative decay, we calculate the product of the Born cross section for $e^+e^- \to \Upsilon_J(1D)\eta$ and the branching fraction for

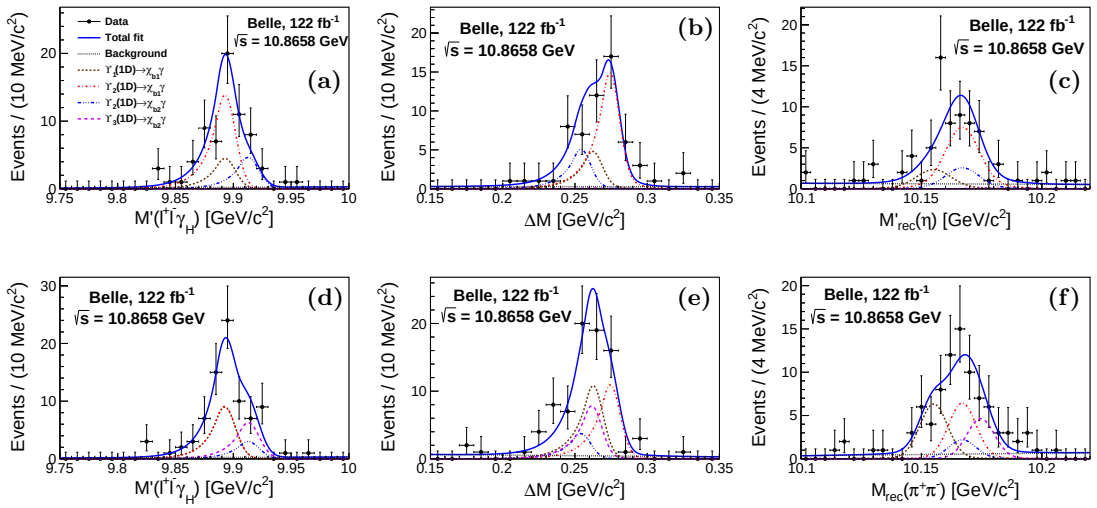


FIG. 1: Distributions of (a) $M'(\ell^+\ell^-\gamma_H)$, (b) ΔM, and (c) $M'_{\rm rec}(\eta)$ in $e^+e^- \to \Upsilon_J(1D)\eta$; and (d) $M'(\ell^+\ell^-\gamma_H)$, (e) ΔM, and (f) $M_{\rm rec}(\pi^+\pi^-)$ in $e^+e^- \to \Upsilon_J(1D)\pi^+\pi^-$ in data at $\sqrt{s} = 10.8658$ GeV with 3D fit results overlaid.

$\Upsilon_J(1D) \to \chi_{b1,b2}\gamma$, using

$$\sigma^{(1)}_{\rm Born} = \frac{N^{\rm sig}\,|1-\Pi|^2}{\mathcal{L}\,\sum_{i=1}^{2}\varepsilon_i\mathcal{B}_i^{\rm int}\,(1+\delta_{\rm ISR})}, \qquad (1)$$

where the index i runs over channels $\eta \to \gamma\gamma$ and $\eta \to \pi^+\pi^-\pi^0$; $\mathcal{L}$ is the integrated luminosity of the data sample; ε_i is the reconstruction efficiency; $\mathcal{B}_i^{\rm int}$ is the product of the branching fractions of all intermediate states. The $(1+\delta_{\rm ISR})$ is the radiative correction factor [22, 34, 35] and the numerical values are listed in the Supplemental Material [33]. In calculating the radiative correction factor, the energy dependency of the Born cross section is described according to the measurement in this work (discussed below). The $|1-\Pi|^2 = 0.93$ at each energy point is the vacuum polarization factor [36, 37]. We calculate $\sigma^{(2)}_{\rm Born}$ for $e^+e^- \to \Upsilon_J(1D)\pi^+\pi^-$ using a similar equation. The values of $\sigma^{(1)}_{\rm Born}$ and $\sigma^{(2)}_{\rm Born}$ are listed in Table I.

Assuming the observed signals are all from $\Upsilon(10860)$ decays, we determine the product of branching fractions of $\Upsilon(10860) \to \Upsilon_J(1D)\eta$ and $\Upsilon_J(1D) \to \chi_{b1,b2}\gamma$ with the following formula

$$\mathcal{B}^{(1)}_{\Upsilon(10860)} = \frac{N^{\rm sig}}{N_{\Upsilon(10860)}\,\sum_{i=1}^{2}\varepsilon_i\mathcal{B}_i^{\rm int}}. \qquad (2)$$

The total number of $\Upsilon(10860)$ events is calculated as $N_{\Upsilon(10860)} = \mathcal{L}\,\sigma(e^+e^- \to b\bar{b}) = (4.2 \pm 0.2) \times 10^7$, where $\sigma(e^+e^- \to b\bar{b}) = 0.34 \pm 0.02$ nb [38]. We calculate the $\mathcal{B}^{(2)}_{\Upsilon(10860)}$ for $e^+e^- \to \Upsilon_J(1D)\pi^+\pi^-$ using a similar equation. The values of $\mathcal{B}^{(1)}_{\Upsilon(10860)}$ and $\mathcal{B}^{(2)}_{\Upsilon(10860)}$ are listed in Table I.

For the other energy points, the $M'_{\rm rec}(\eta)$ and $M_{\rm rec}(\pi^+\pi^-)$ distributions after applying the signal region requirements of $9.83 < M'(\ell^+\ell^-\gamma_H) < 9.94$ GeV/c^2 and $0.20 < \Delta M < 0.29$ GeV/c^2 (about 98% of signal candidates are retained) are shown in the Supplemental Material [33]. These distributions are very sparse and, instead of fitting, we use event counting. We combine the $\Upsilon_1(1D)$, $\Upsilon_2(1D)$, and $\Upsilon_3(1D)$ states due to significant cross-feed among them.

We count the number of events, $N^{\rm obs}$, in the $\Upsilon_J(1D)$ signal region of (10.13 – 10.19) GeV/c^2. The signal yield is defined as $N^{\rm sig} = \max(0, N^{\rm obs} - N^{\rm bg})$. To determine the number of background events, $N^{\rm bg}$, we perform a 3D fit to the data sample that combines all energies, including 10.866 GeV. At all energy points except $\sqrt{s}$ = 10.866 GeV, the total numbers of $N^{\rm obs}$ and $N^{\rm bg}$ in $e^+e^- \to \Upsilon_J(1D)\eta$ ($e^+e^- \to \Upsilon_J(1D)\pi^+\pi^-$) are 3.0 (8.0) and 1.7 (1.4), respectively. The background is assumed to be of non-resonant origin, and for each energy, the $N^{\rm bg}$ value is assigned based on the corresponding luminosity and the background yield in the combined sample. The statistical uncertainties on $N^{\rm sig}$ are assigned based on 68.3% confidence intervals provided by the Poissonian limit estimator (POLE) program [39]; these are equivalent to the unified approach in Ref. [40].

The product of the Born cross section for $e^+e^- \to \Upsilon_J(1D)\eta$, the branching fraction for $\Upsilon_J(1D) \to \chi_{b1,b2}\gamma$, and the branching fraction for $\chi_{b1,b2} \to \Upsilon(1S)\gamma$ ($\sigma^{(3)}_{\rm Born}$) is calculated using Eq. (1), where $\mathcal{B}_i^{\rm int} = \mathcal{B}(\eta \to \gamma\gamma)\,\mathcal{B}(\Upsilon(1S) \to \ell^+\ell^-)$ or $\mathcal{B}(\eta \to \pi^+\pi^-\pi^0)\,\mathcal{B}(\pi^0 \to \gamma\gamma)\,\mathcal{B}(\Upsilon(1S) \to \ell^+\ell^-)$. We calculate the corresponding $\sigma^{(4)}_{\rm Born}$ for $e^+e^- \to \Upsilon_J(1D)\pi^+\pi^-$ using a similar equation. At $\sqrt{s} = 10.866$ GeV, we use the same counting method to determine $\sigma^{(3)}_{\rm Born}$ and $\sigma^{(4)}_{\rm Born}$. The upper limits are calculated directly using POLE, with the same configuration as in Ref. [28]. The signal yields, Born cross sections, and upper limits on the Born cross sections are

TABLE I: Results for $e^+e^- \to \Upsilon_J(1D)\eta$ and $e^+e^- \to \Upsilon_J(1D)\pi^+\pi^-$ at $\sqrt{s} = 10865.8$ MeV. All symbols are explained in the text.

Channel	$\varepsilon_{\eta\to\gamma\gamma,\eta\to\pi^+\pi^-\pi^0}$	$N^{\rm sig}$	$\mathcal{B}^{(1)}_{\Upsilon(10860)}(\times10^{-3})$	$\sigma^{(1)}_{\rm Born}$(pb)
$e^+e^- \to \Upsilon_1(1D)\eta$, $\Upsilon_1(1D) \to \chi_{b1}\gamma$	0.102, 0.041	12.2 ± 6.3	$0.34 \pm 0.18 \pm 0.06$	$0.17 \pm 0.09 \pm 0.03$
$e^+e^- \to \Upsilon_2(1D)\eta$, $\Upsilon_2(1D) \to \chi_{b1}\gamma$	0.103, 0.042	37.8 ± 8.0	$1.05 \pm 0.22 \pm 0.12$	$0.52 \pm 0.11 \pm 0.06$
$e^+e^- \to \Upsilon_2(1D)\eta$, $\Upsilon_2(1D) \to \chi_{b2}\gamma$	0.103, 0.042	12.9 ± 6.0	$0.70 \pm 0.33 \pm 0.18$	$0.34 \pm 0.17 \pm 0.09$
$e^+e^- \to \Upsilon_3(1D)\eta$, $\Upsilon_3(1D) \to \chi_{b2}\gamma$	0.104, 0.043	0.3 ± 2.8	$0.02 \pm 0.15 \pm 0.02$	$0.01 \pm 0.07 \pm 0.01$
Channel	$\varepsilon_{\pi^+\pi^-}$	$N^{\rm sig}$	$\mathcal{B}^{(2)}_{\Upsilon(10860)}(\times10^{-3})$	$\sigma^{(2)}_{\rm Born}$(pb)
$e^+e^- \to \Upsilon_1(1D)\pi^+\pi^-$, $\Upsilon_1(1D) \to \chi_{b1}\gamma$	0.177	24.7 ± 6.5	$0.19 \pm 0.05 \pm 0.03$	$0.09 \pm 0.02 \pm 0.01$
$e^+e^- \to \Upsilon_2(1D)\pi^+\pi^-$, $\Upsilon_2(1D) \to \chi_{b1}\gamma$	0.180	25.0 ± 6.7	$0.19 \pm 0.06 \pm 0.03$	$0.09 \pm 0.03 \pm 0.01$
$e^+e^- \to \Upsilon_2(1D)\pi^+\pi^-$, $\Upsilon_2(1D) \to \chi_{b2}\gamma$	0.181	8.5 ± 4.2	$0.13 \pm 0.06 \pm 0.04$	$0.06 \pm 0.03 \pm 0.02$
$e^+e^- \to \Upsilon_3(1D)\pi^+\pi^-$, $\Upsilon_3(1D) \to \chi_{b2}\gamma$	0.182	17.9 ± 6.7	$0.27 \pm 0.09 \pm 0.03$	$0.13 \pm 0.05 \pm 0.02$

listed in the Supplemental Material [33].

The systematic uncertainties in the measurements of cross sections for $e^+e^- \to \Upsilon_J(1D)\eta$ and $e^+e^- \to \Upsilon_J(1D)\pi^+\pi^-$ include contributions from the photon energy calibration, fit model, reconstruction efficiency, radiative correction factor, angular distributions, beam-energy calibration, trigger simulation, integrated luminosity, and branching fractions of intermediate states. The additive systematic uncertainties are those from the photon energy calibration and fit model. The other sources of systematic uncertainties are multiplicative.

We study the additive systematic uncertainties from the photon energy calibration and fitting procedure as follows. The resulting uncertainties of the peak positions are 1.1 MeV/c^2 in both the $M'(\ell^+\ell^-\gamma_H)$ and ΔM distributions; the uncertainties in the resolutions are 0.9 and 1.1 MeV/c^2 in the $M'(\ell^+\ell^-\gamma_H)$ and ΔM distributions [29]. For the results obtained with the fitting method, we change the signal peak positions and resolutions by $\pm1\sigma$. We increase the order of the polynomial describing the background by one and change the fit interval. We vary the ratio $N^{\rm sig}(\eta \to \gamma\gamma)/N^{\rm sig}(\eta \to \pi^+\pi^-\pi^0)$ from 4.2 to 4.0 and 4.4 to account for the uncertainties of the efficiencies and the η decay branching fractions, and take the difference in the yield as a systematic uncertainty. For each fitted quantity, we varied all the above configurations simultaneously and conservatively consider the largest deviation from the nominal result as the additive systematic uncertainty for the corresponding energy point.

The contributions to the multiplicative systematic uncertainty are given in Table II. Detection efficiency uncertainties include momentum-dependent tracking uncertainties (1.0% per pion and 0.4% per lepton, derived from $D^{*+} \to D^0(\to K^0_S\pi^+\pi^-)\pi^+$), pion identification (1.1% per pion, derived from $D^{*+} \to D^0(\to K^-\pi^+)\pi^+$), lepton identification (1.6% per electron and 1.2% per muon, derived from $\gamma\gamma \to \ell^+\ell^-$ ($\ell = {\rm e}, \mu$)), photon reconstruction (2.0% per photon, derived from $e^+e^- \to \gamma e^+e^-$), and π^0 reconstruction (2.3% per π^0, derived from $\tau^- \to \pi^-\pi^0\nu_\tau$).

TABLE II: The multiplicative systematic uncertainties (%) in the measurements of cross sections for $e^+e^- \to \Upsilon_J(1D)\eta$ and $e^+e^- \to \Upsilon_J(1D)\pi^+\pi^-$.

Source	$\Upsilon_J(1D)\eta$	$\Upsilon_J(1D)\pi^+\pi^-$
Efficiency	8.6	6.2
Angular distributions	1.7	6.6
Radiative correction factor	2.0	6.3
Luminosity	1.4	1.4
Branching fractions	6.7	6.6
Total	11.3	12.9

When the uniform angular distributions are changed to $1 \pm \cos^2\theta_\eta$ and $1 \pm \cos^2\theta_{\pi^+\pi^-}$, the maximal deviations in the efficiency are 1.7% and 4.8% for $e^+e^- \to \Upsilon_J(1D)\eta$ and $e^+e^- \to \Upsilon_J(1D)\pi^+\pi^-$ [41], respectively. We assume a flat distribution of θ_{π^+} in the $\pi^+\pi^-$ system in $e^+e^- \to \Upsilon_J(1D)\pi^+\pi^-$. We change the uniform distribution to $1 \pm \cos^2\theta_{\pi^+}$, and take the maximal deviation of 4.5% in the efficiency as the systematic uncertainty due to angular distribution. The trigger uncertainty is neglected because the trigger efficiencies for $e^+e^- \to \Upsilon_J(1D)\eta$ and $e^+e^- \to \Upsilon_J(1D)\pi^+\pi^-$ are 99.3% and 100.0%.

The uncertainties in the center of mass energies are about 1 MeV. We change the collision energies in the 5C kinematic fit by $\pm1\sigma$ and find the deviations in the signal yields are less than 1.0%, which is negligible. In calculating the radiative correction factor, the measured energy dependence of the cross sections is used. We change all of the parameters in the fit function by $\pm1\sigma$ according to the fitted results from the distributions of $\sigma(e^+e^- \to \Upsilon_J(1D)\eta)$ and $\sigma(e^+e^- \to \Upsilon_J(1D)\pi^+\pi^-)$ as a function of e^+e^- c.m. energy, and take the maximum difference on the radiative correction factor as the resulting uncertainty. Belle measures luminosity at 1.4% precision using wide angle Bhabha events. The branching fractions of all intermediate decays are taken from Ref. [26]. We add all the multiplicative systematic uncertainties in quadrature to obtain the final multiplicative systematic uncertainty, as listed in Table II.

We perform all possible combinations of the above variations of the fit, and conservatively consider the largest deviation of fit results as the systematic uncertainty in the measurement of $\Upsilon_J(1D)$ masses. The uncertainty due to the fit interval is dominant.

The dressed cross sections ($\sigma_{\rm dressed}$) for $e^+e^- \to \Upsilon_J(1D)\eta$ or $e^+e^- \to \Upsilon_J(1D)\pi^+\pi^-$ as a function of c.m. energy are shown in Fig. 2. The $\sigma_{\rm dressed}$ can be obtained by removing the vacuum polarization factor. The triangles show the dressed cross sections for $e^+e^- \to \Upsilon_J(1D)\pi^+\pi^-$ at Belle II, which are obtained according to the recoil mass distributions of $\pi^+\pi^-$ [42] (see the Supplemental Material [33] for details). The profile likelihoods for each energy point are given in the Supplemental Material [33]. The fit function to the Belle and Belle II data points is the sum of the phase-space and a coherent sum of the $\Upsilon(10860)$ and $\Upsilon(11020)$ Breit-Wigner amplitudes:

$$\Big|\sum_{i=1}^{2}\frac{\sqrt{12\pi\Gamma_{ee,i}\mathcal{B}_i\Gamma_i}}{s-M_i^2-iM_i\Gamma_i}\sqrt{\frac{\Phi(\sqrt{s})}{\Phi(M_i)}}e^{i\phi}\Big|^2+c_{\rm NR}\Phi(\sqrt{s}), \quad (3)$$

where the index i runs over the $\Upsilon(10860)$ and $\Upsilon(11020)$ states; M_i, Γ_i, and $\Gamma_{ee,i}$ are the mass, total width, and electronic width of the Υ states; Φ is the phase-space factor; ϕ is the complex phase; and $c_{\rm NR}$ is a constant. Only one solution is found from the fit since the interference is weak due to the large mass difference between the $\Upsilon(10860)$ and $\Upsilon(11020)$ and the insignificant signal of the $\Upsilon(11020)$. Their masses and widths are fixed to the world-average values [26]. The parameters $\Gamma_{ee,i}\mathcal{B}_i$ and ϕ are floated. The fitted results are shown in Fig. 2 and summarized in Table III. Since the signal significances of fit outputs are less than 3σ, the upper limits at 90% C.L. are also given in Table III. The value of ϕ is (-0.5 ± 0.6) rad for $e^+e^- \to \Upsilon_J(1D)\pi^+\pi^-$. Systematic uncertainties in the cross section energy dependence fit results include the beam-energy calibration, the fit model, and the multiplicative systematic uncertainties of cross section measurements [28]. For $e^+e^- \to \Upsilon_J(1D)\pi^+\pi^-$, the Belle and Belle II-specific correlated multiplicative uncertainties are taken into account separately [28]. The uncertainties from the masses and widths of the $\Upsilon(10860)$ and $\Upsilon(11020)$ are dominant.

TABLE III: Fitted values for $\Gamma_{ee}\mathcal{B}(\Upsilon(10860,11020) \to \Upsilon_J(1D)\eta)\mathcal{B}_f$ and $\Gamma_{ee}\mathcal{B}(\Upsilon(10860,11020) \to \Upsilon_J(1D)\pi^+\pi^-)\mathcal{B}_f$ in eV, where $\mathcal{B}_f = \mathcal{B}(\Upsilon_J(1D) \to \chi_{b1,b2}\gamma)\mathcal{B}(\chi_{b1,b2} \to \Upsilon(1S)\gamma)$. The upper limits at 90% C.L. are shown in square brackets.

$\Gamma_{ee}\mathcal{B}(\Upsilon(10860) \to \Upsilon_J(1D)\eta)\mathcal{B}_f$	$(0.091 \pm 0.039 \pm 0.016)$ [< 0.14]
$\Gamma_{ee}\mathcal{B}(\Upsilon(11020) \to \Upsilon_J(1D)\eta)\mathcal{B}_f$	$(0.000 \pm 0.018 \pm 0.005)$ [< 0.04]
$\Gamma_{ee}\mathcal{B}(\Upsilon(10860) \to \Upsilon_J(1D)\pi^+\pi^-)\mathcal{B}_f$	$(0.034 \pm 0.013 \pm 0.006)$ [< 0.06]
$\Gamma_{ee}\mathcal{B}(\Upsilon(11020) \to \Upsilon_J(1D)\pi^+\pi^-)\mathcal{B}_f$	$(0.020 \pm 0.016 \pm 0.005)$ [< 0.05]

In summary, we measure the cross sections for $e^+e^- \to \Upsilon_J(1D)\eta$ and $e^+e^- \to \Upsilon_J(1D)\pi^+\pi^-$ using Belle data collected at c.m. energies between 10.73 and 11.02 GeV.

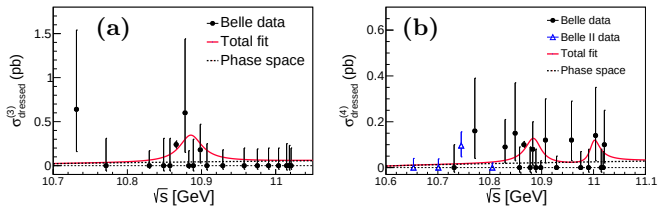


FIG. 2: Energy dependences of (a) $\sigma^{(3)}_{\rm dressed}$ and (b) $\sigma^{(4)}_{\rm dressed}$ for $e^+e^- \to \Upsilon_J(1D)\eta$ and $e^+e^- \to \Upsilon_J(1D)\pi^+\pi^-$. Filled circles show the measurements at Belle, and triangles show the measurements at Belle II [42]. Error bars represent the total uncorrelated uncertainties (statistical and additive uncertainties). Curves show the fit results to the Belle and Belle II data points.

We report first evidence for the $\Upsilon_1(1D)$ and $\Upsilon_3(1D)$ states. In the η channel, $\Upsilon_3(1D)$ production is strongly suppressed and $\Upsilon_1(1D)$ production is slightly suppressed relative to $\Upsilon_2(1D)$, which is consistent with the prediction in Ref. [11]. In the $\pi^+\pi^-$ channel, however, we find comparable production rates for the $\Upsilon_1(1D)$, $\Upsilon_2(1D)$, and $\Upsilon_3(1D)$ states. The mass for $\Upsilon_2(1D)$ is $(10167.0 \pm 1.0 \pm 0.2)$ MeV/c^2. We compare the mass splittings Δm_{12} and Δm_{23} with different theoretical predictions, as shown in Fig. 3.

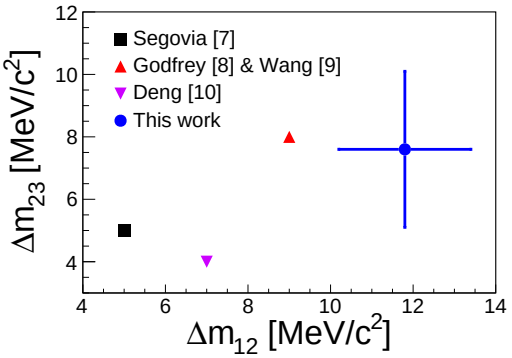


FIG. 3: The comparison of mass splittings Δm_{12} and Δm_{23} with different theoretical predictions. The predictions are derived from nonrelativistic constituent quark model in Segovia [7], relativized quark model in Godfrey [8], the modified relativized quark model with a screening effect in Wang [9], and screened potential model in Deng [10]. The correlation coefficient between Δm_{12} and Δm_{23} is -0.06.

This work, based on data collected using the Belle detector, which was operated until June 2010, was supported by the Ministry of Education, Culture, Sports, Science, and Technology (MEXT) of Japan, the Japan Society for the Promotion of Science (JSPS), and the Tau-Lepton Physics Research Center of Nagoya University; the Australian Research Council including grants DP210101900, DP210102831, DE220100462, LE210100098, LE230100085; Austrian Federal Ministry of Education, Science and Research (FWF)

and FWF Austrian Science Fund No. P 31361-N36; National Key R&D Program of China under Contract No. 2022YFA1601903, 2024YFA1610503, and 2024YFA1610504; National Natural Science Foundation of China and research grants No. 12475076, No. 11575017, No. 11761141009, No. 11705209, No. 11975076, No. 12135005, No. 12150004, No. 12161141008, and No. 12175041, and Shandong Provincial Natural Science Foundation Project ZR2022JQ02; Fundamental Research Funds of China for the Central Universities under contract Nos. 2242025RCB0014 and RF1028623046; the Czech Science Foundation Grant No. 22-18469S; Horizon 2020 ERC Advanced Grant No. 884719 and ERC Starting Grant No. 947006 "InterLeptons" (European Union); the Carl Zeiss Foundation, the Deutsche Forschungsgemeinschaft, the Excellence Cluster Universe, and the VolkswagenStiftung; the Department of Atomic Energy (Project Identification No. RTI 4002), the Department of Science and Technology of India, and the UPES (India) SEED finding programs Nos. UPES/R&D-SEED-INFRA/17052023/01 and UPES/R&D-SOE/20062022/06; the Istituto Nazionale di Fisica Nucleare of Italy; National Research Foundation (NRF) of Korea Grants No. 2021R1-F1A-1064008, No. 2022R1-A2C-1003993, No. RS-2018-NR031074, No. RS-2021-NR060129, No. RS-2024-00354342 No. RS-2025-02219521, No. RS-2026-25471491, No. RS-2026-25480677, and No. RS-2026-25486791, Radiation Science Research Institute, Foreign Large-Size Research Facility Application Supporting project, the Global Science Experimental Data Hub Center, the Korea Institute of Science and Technology Information (K26L1M2C3) and KREONET/GLORIAD; the Polish Ministry of Science and Higher Education and the National Science Center; the Ministry of Science and Higher Education of the Russian Federation and the HSE University Basic Research Program, Moscow; University of Tabuk research grants S-1440-0321, S-0256-1438, and S-0280-1439 (Saudi Arabia); the Slovenian Research Agency Grant Nos. J1-50010 and P1-0135; Ikerbasque, Basque Foundation for Science, and the State Agency for Research of the Spanish Ministry of Science and Innovation through Grant No. PID2022-136510NB-C33 (Spain); the Swiss National Science Foundation; the Ministry of Education and the National Science and Technology Council of Taiwan; and the United States Department of Energy and the National Science Foundation. These acknowledgements are not to be interpreted as an endorsement of any statement made by any of our institutes, funding agencies, governments, or their representatives. We thank the KEKB group for the excellent operation of the accelerator; the KEK cryogenics group for the efficient operation of the solenoid; and the KEK computer group and the Pacific Northwest National Laboratory (PNNL) Environmental Molecular Sciences Laboratory (EMSL) computing group for strong computing support; and the National Institute of Informatics, and Science Information NETwork 6 (SINET6) for valuable network support.

Numerical data corresponding to the results presented are available as HEPData. The full Belle II data are not publicly available. The collaboration will consider requests for access to the data that support this article.

[1] N. Brambilla *et al.*, Eur. Phys. J. C **71**, 1534 (2011).
[2] N. Brambilla *et al.*, Eur. Phys. J. C **74**, 2981 (2014).
[3] X. C. Dai, S. Jia, A. Nefediev, J. Nieves, C. P. Shen, and L. M. Zhang, arXiv:2603.09315.
[4] N. Brambilla *et al.*, CERN Yellow Reports: Monographs, arXiv:hep-ph/0412158.
[5] G. Bonvicini *et al.* (CLEO Collaboration), Phys. Rev. D **70**, 032001 (2004).
[6] P. del Amo Sanchez *et al.* (BaBar Collaboration), Phys. Rev. D **82**, 111102 (2010).
[7] J. Segovia, P.G. Ortega, D.R. Entem, and F. Fernández, Phys. Rev. D **93**, 074027 (2016).
[8] S. Godfrey and K. Moats, Phys. Rev. D **92**, 054034 (2015).
[9] J. Z. Wang, Z. F. Sun, X. Liu, and T. Matsuki, Eur. Phys. J. C **78**, 915 (2018).
[10] W. J. Deng, H. Liu, L. C. Gui, and X. H. Zhong, Phys. Rev. D **95**, 074002 (2017).
[11] B. Wang, X. Liu, and D. Y. Chen, Phys. Rev. D **94**, 094039 (2016).
[12] Q. Huang, H. Xu, X. Liu, and T. Matsuki, Phys. Rev. D **97**, 094018 (2018).
[13] Q. Wu, D. Y. Chen, and T. Matsuki, Phys. Rev. D **102**, 114037 (2020).
[14] U. Tamponi *et al.* (Belle Collaboration), Eur. Phys. J. C **78**, 633 (2018).
[15] I. Adachi *et al.* (Belle Collaboration), Phys. Rev. Lett. **108**, 032001 (2012).
[16] A. Abashian *et al.* (Belle Collaboration), Nucl. Instr. and Methods Phys. Res. Sect. A **479**, 117 (2002).
[17] Jolanta Brodzicka *et al.* (Belle Collaboration), Prog. Theor. Exp. Phys. **2012**, 04D001 (2012).
[18] S. Kurokawa and E. Kikutani, Nucl. Instr. and Methods Phys. Res. Sect. A **499**, 1 (2003), and other papers included in this volume.
[19] T. Abe *et al.*, Prog. Theor. Exp. Phys. **2013**, 03A001 (2013), and references therein.
[20] D. J. Lange, Nucl. Instr. and Methods Phys. Res. Sect. A **462**, 152 (2001).
[21] G. Rodrigo, H. Czyż, J. H. Kühn, and M. Szopa, Eur. Phys. J. C **24**, 71 (2002).
[22] S. Jadach, B. F. L. Ward, and Z. Was, Phys. Rev. D **63**, 113009 (2001); Comput. Phys. Commun. **130**, 260 (2000).
[23] R. Brun *et al.*, *GEANT*, CERN Report No. DD/EE/84-1 (1984).

[24] J. P. Lees *et al.* (BaBar Collaboration), Phys. Rev. D **90**, 112010 (2014).
[25] M. Kornicer *et al.* (CLEO Collaboration), Phys. Rev. D **83**, 054003 (2011).
[26] S. Navas *et al.* (Particle Data Group), Phys. Rev. D **110**, 030001 (2024) and 2025 update.
[27] R. Mizuk *et al.* (Belle Collaboration), JHEP **10** (2019) 220.
[28] I. Adachi *et al.* (Belle II Collaboration), JHEP **04** (2026) 101.
[29] R. Mizuk *et al.* (Belle and Belle II Collaborations), Phys. Rev. Lett. **109**, 232002 (2012).
[30] T. Kuhr, C. Pulvermacher, M. Ritter, T. Hauth, and N. Braun, Comput. Softw. Big Sci. **3**, 1 (2019).
[31] T. Skwarnicki, Ph.D. thesis, Institute for Nuclear Physics, 1986; DESY Report No. DESY F31-86-02, 1986.
[32] S. S. Wilks, Annals Math. Statist. **9**, 60 (1938).
[33] See Supplemental Material at [URL will be inserted by publisher] for additional information.
[34] E. A. Kuraev and V. S. Fadin, Yad. Fiz. **41**, 733 (1985) [Sov. J. Nucl. Phys. **41**, 466 (1985)].
[35] M. Benayoun, S. I. Eidelman, V. N. Ivanchenko, and Z. K. Silagadze, Mod. Phys. Lett. A **14**, 2605 (1999).
[36] X. K. Dong, X. H. Mo, P. Wang, and C. Z. Yuan, Chin. Phys. C **44**, 083001 (2020).
[37] S. Actis *et al.* (Working Group on Radiative Corrections and Monte Carlo Generators for Low Energies Collaborations), Eur. Phys. J. C **66**, 585 (2010).
[38] S. Esen *et al.* (Belle Collaboration), Phys. Rev. D **87**, 031101 (2013).
[39] J. Conrad, O. Botner, A. Hallgren, and C. Perez de los Heros, Phys. Rev. D **67**, 012002 (2003).
[40] G. J. Feldman and R. D. Cousins, Phys. Rev. D **57**, 3873 (1998).
[41] Y. Tosa, Report No. DPNU-34-1976, 1976, http://inspirehep.net/record/109354.
[42] M. Abumusabh *et al.* (Belle II Collaboration), JHEP **06** (2026) 278.